Advanced Composite Materials
Publication details, including instructions for authors and subscription information:
http://www.tandfonline.com/loi/tacm20

Suppression of interfacial crack for foam core sandwich panel with crack arrester

Y. Hirose [a], M. Hojo [b], A. Fujiyoshi [c] & G. Matsubara [d]

[a] Commercial Aircraft Project Engineering Division, Aerospace Company, Kawasaki Heavy Industries, Ltd, 1. Kawasaki-cho, Kakamigahara City, Gifu-Pref. 504-8710, Japan

[b] Department of Mechanical Engineering and Science, Kyoto University, Sakyo-ku, Kyoto City, Kyoto Pref. 606-8501, Japan

[c] Department of Mechanical Engineering and Science, Kyoto University, Sakyo-ku, Kyoto City, Kyoto Pref. 606-8501, Japan

[d] Strength Research Department, Technical Institute, Kawasaki Heavy Industries, Ltd, 1. Kawasaki-Cho, Akashi City, Hyogo-Pref. 673-8666, Japan

Version of record first published: 02 Apr 2012.

To cite this article: Y. Hirose , M. Hojo , A. Fujiyoshi & G. Matsubara (2007): Suppression of interfacial crack for foam core sandwich panel with crack arrester, Advanced Composite Materials, 16:1, 11-30

To link to this article: http://dx.doi.org/10.1163/156855107779755309

Adv. Composite Mater., Vol. 16, No. 1, pp. 11–30 (2007)

Also available online - www.brill.nl/acm

Suppression of interfacial crack for foam core sandwich panel with crack arrester

Y. HIROSE [1,*], M. HOJO [2], A. FUJIYOSHI [2] and G. MATSUBARA [3]

[1] *Commercial Aircraft Project Engineering Division, Aerospace Company, Kawasaki Heavy Industries, Ltd, 1. Kawasaki-cho, Kakamigahara City, Gifu-Pref. 504-8710, Japan*
[2] *Department of Mechanical Engineering and Science, Kyoto University, Sakyo-ku, Kyoto City, Kyoto Pref. 606-8501, Japan*
[3] *Strength Research Department, Technical Institute, Kawasaki Heavy Industries, Ltd, 1. Kawasaki-Cho, Akashi City, Hyogo-Pref. 673-8666, Japan*

Received 22 September 2005; accepted 24 February 2006

Abstract—Since delamination often propagates at the interfacial layer between a surface skin and a foam core, a crack arrester is proposed for the suppression of the delamination. The arrester has a semi-cylindrical shape and is arranged in the foam core and is attached to the surface skin. Here, energy release rates and complex stress intensity factors are calculated using finite element analysis. Effects of the arrester size and its elastic moduli on the crack suppressing capability are investigated. Considerable reductions of the energy release rates at the crack tip are achieved as the crack tip approached the leading edge of the crack arrester. Thus, this new concept of a crack arrester may become a promising device to suppress crack initiation and propagation of the foam core sandwich panels.

Keywords: Foam core; sandwich structure; new crack arrester; delamination suppression; fracture mechanics; energy release rate.

1. INTRODUCTION

Almost all Modern commercial aircrafts use carbon fiber reinforced plastic (CFRP) as a primary structural material since the early 1980s [1, 2]. CFRP material is to be applied to the primary structure of the main wing and fuselage for the next generation transports. The structural weight fraction of the CFRP is expected to exceed 50%. However, the structural design concept of these commercial transports will remain a conventional one, consisting of skins, stringers and frames for a

Edited by the JSCM.

*To whom correspondence should be addressed. E-mail: hirose_yasuo@khi.co.jp

fuselage structure. Innovative structural concepts should be investigated to use the full potential capability of the composite materials for weight and part count reduction. The foam core sandwich panel structure is one of the most promising candidates [3–5]. Various authors have carried out fundamental research for this structural concept [6, 7]. As for current industrial applications, the foam core sandwich panel is used in rolling stocks, a maritime application and it is also used in building construction. The Japanese bullet train, Shinkansen, E4 type [8] and Swedish corvette, Visby [9], are typical examples. As for the primary structures for aerospace industries, authors have conducted research activities to apply the foam core sandwich panel structure, which consists of CFRP surface skins and the polyetherimide (PEI) core, to the nose structure of the commercial transport under the contract of the Japanese Government, New Energy and Industrial Technologies Development Organization (NEDO) [10, 11]. Considerable weight and part-count reduction was achieved compared with conventional metal structures in this research. It was also pointed out that suppression of crack propagation between the surface skin and the foam core was the critical issue to improve the damage tolerance capability of this concept. The interfacial crack propagation behavior was investigated in our preliminary experiment. The crack propagation path remained in the interfacial layer between the CFRP surface skin and the foam core. This fact led to the idea that stiff material just below the surface skin could prevent crack propagations.

With this point of view, the authors devised a new crack arrester concept to suppress the interfacial crack propagation. In the present study, a co-cured semi-cylindrical crack arrester, located on the interface between the surface skin and the foam core, was evaluated. The effects of the crack arrester on the energy release rates at the crack tip were estimated for Mode I and Mode II loading conditions.

2. FOAM CORE SANDWICH PANEL

2.1. Description of the foam core sandwich panel specimen

Foam core sandwich panel specimens consisted of two materials: CFRP (Toho Tenax UT500/#135, graphite/epoxy twill weave fabric prepreg), PEI (polyetherimide) foam core. The PEI foam core was placed between CFRP surface skins. The ply-orientations of the CFRP surface skin were $(+45, -45)/(0, 90)$ with nominal thickness of 0.92 mm. The size of the specimen was 300 mm $\times$ 100 mm $\times$ 35 mm thickness. Surface skins and the core were co-cured without adhesive. Overviews of the specimen along with a detailed construction sketch are shown in Figs 1 and 2, respectively. Mechanical properties of the surface skin and the PEI core are summarized in Table 1.

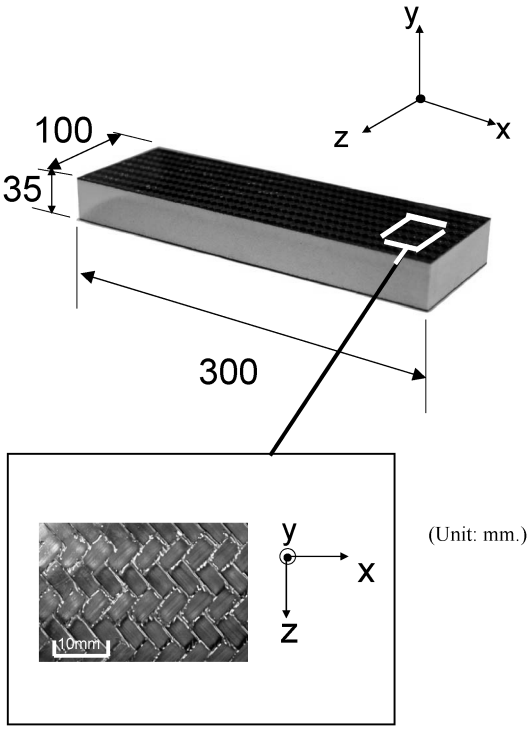

Figure 1. Foam core sandwich panel specimen.

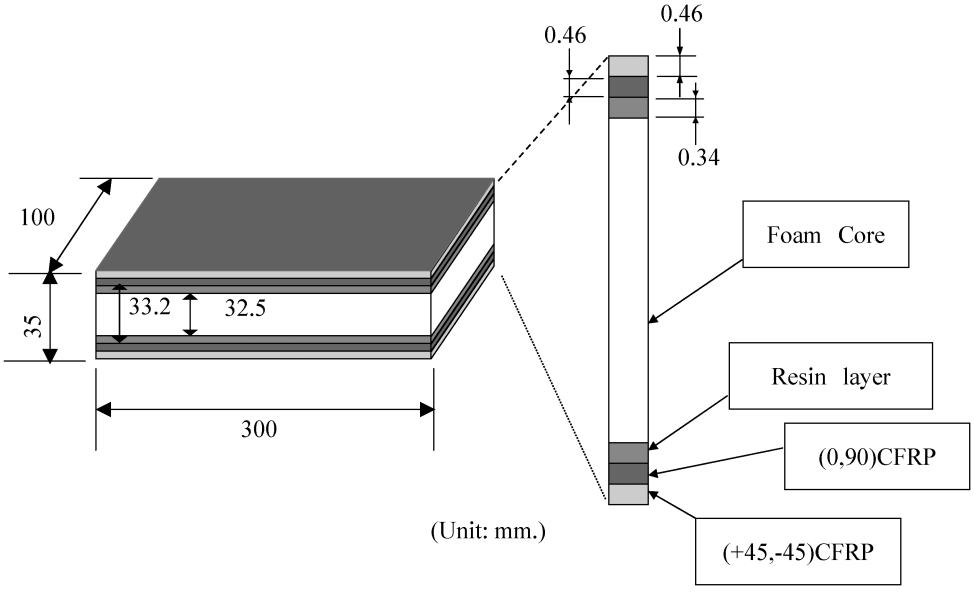

Figure 2. Schematic view of the construction of foam core sandwich panel for FE analysis.

Table 1.
Material properties of foam core sandwich panel

Material properties	Resin	PEI core
E (GPa)	4.10	2.75×10^{-2}
ν	0.330	0.250
G (GPa)	1.54	1.10×10^{-2}

Material properties	CFRP (+45, −45)	CFRP (0, 90)	CFRP (90)
E_{11} (GPa)	12.6	54.9	8.61
E_{22} (GPa)	8.61	8.61	8.61
E_{33} (GPa)	12.6	54.9	127
ν_{12}	0.330	0.330	0.550
ν_{23}	0.230	5.20×10^{-2}	2.20×10^{-2}
ν_{31}	0.780	0.051	0.330
G_{12} (GPa)	3.31	3.77	2.78
G_{23} (GPa)	3.31	3.77	4.23
G_{31} (GPa)	26.1	3.53	4.23

2.2. Micro-structure of foam core sandwich panel and fracture behavior

A microscopic observation by a special microscope VH-700 (Keyence digital HD) with zoom lens (75–750 times) revealed that resin from the surface skins impregnated into cells of the foam core adjacent to the skin, and the thickness of the resin layer was about 0.34 mm (see Fig. 3). The macroscopic photo of the propagated crack is shown in Fig. 4(a) and attached core cells on the surface skin were observed in Fig. 4(b). A similar result was reported by another author [7]. Photographs indicated that the interfacial crack is propagated between this resin-impregnated layer and the original foam core through the preliminary test under the Mode I loading condition.

2.3. Concept of the new crack arrester of foam core sandwich panel

Since the interfacial crack propagates between the resin layer and the foam core, a dissimilar material with higher stiffness, installed on the crack propagation path, is expected to suppress the crack propagation. This concept of a crack arrester is shown in Fig. 5. Crack arresters with semi-cylindrical shapes are arranged between the CFRP surface skin and the foam core considering the production efficiency. Here, the straight portion of the arrester was attached to the surface skin. The material of the crack arrester should have a higher modulus than that of the foam core material. Candidates for the arrester materials are CFRP (Toho Tenax UT500/#135) and an epoxy resin. The fiber direction is perpendicular to the

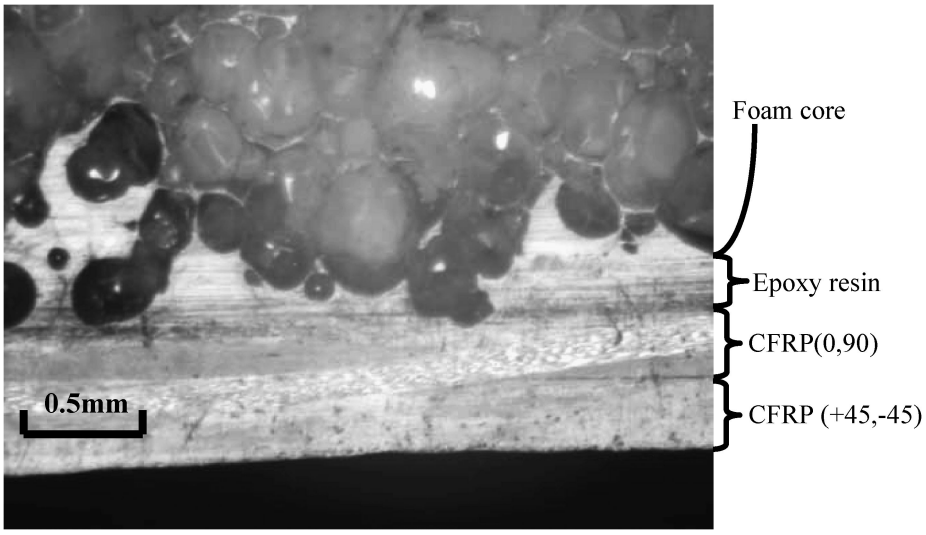

Figure 3. Optical micrograph around interface between skin and core.

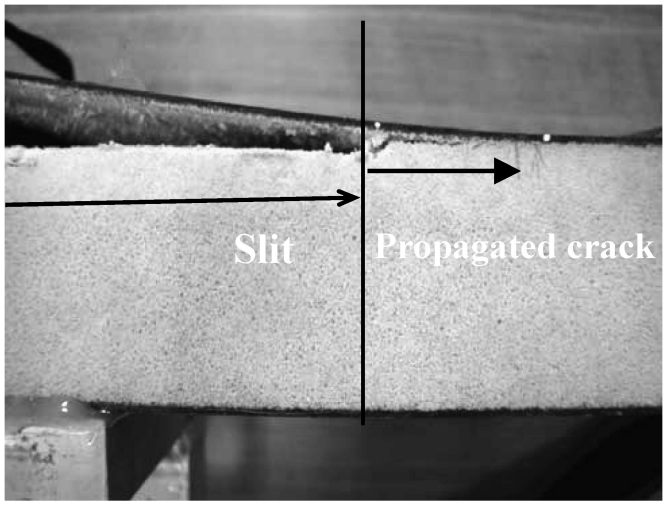

(a) Propagated crack in DCB test

Figure 4. Interfacial crack propagation for foam core sandwich panel.

crack propagation direction in the case of the CFRP material. If the crack arrester decreases the energy release rates at the crack tip below the fracture toughness value of the skin-core interface, the crack will be suppressed or stopped. This crack suppression effect of the arrester is estimated analytically in the following sections.

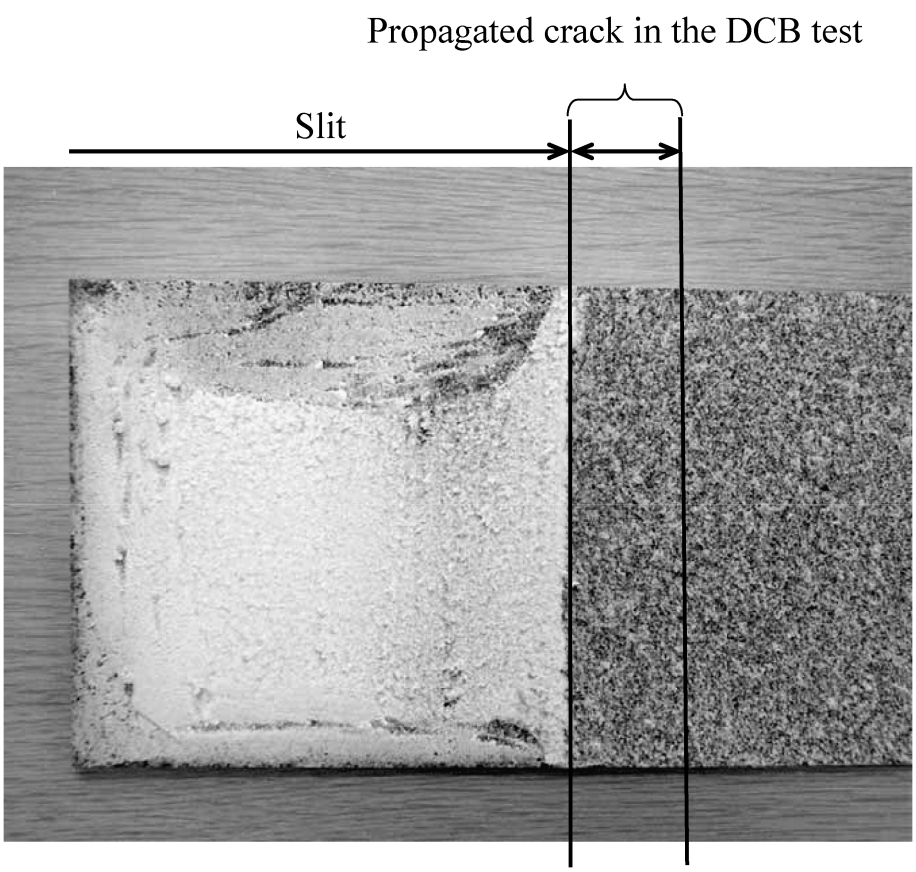

Figure 4. Continued.

3. ANALYTICAL METHOD

3.1. Introduction of fracture mechanical parameters

3.1.1. Theoretical solutions for distribution of stress and displacement near the interfacial crack tip. The theoretical analyses for stress and displacement distribution near the interfacial crack tip between two dissimilar materials are shown below in order to define the fracture mechanical parameters. Materials are described as indexes 1 and 2. E_i, μ_i, and ν_i express Young's modulus, shear modulus and Poisson's ratio, respectively. The distance from the crack tip is described as r.

The relation between stress σ_{ij} and r near the crack tip is shown in the following equations

$$\sigma_{ij} \propto r^{\lambda}. \tag{1}$$

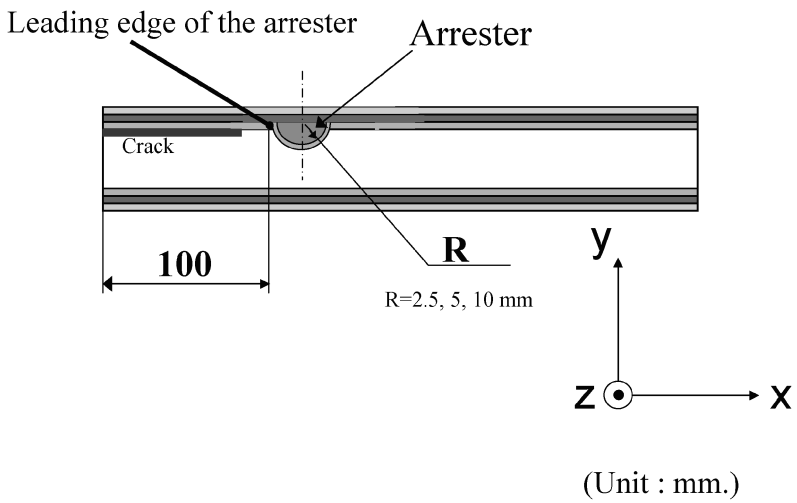

Figure 5. Schematic view of FE Model for crack arrester (in front of the leading edge).

The parameter ε is introduced as a constant depending on the combination of two materials and is defined by the following equation [12]:

$$\varepsilon = \frac{1}{2\pi} \ln\left[\frac{\frac{\chi_1}{\mu_1} + \frac{1}{\mu_2}}{\frac{\chi_2}{\mu_2} + \frac{1}{\mu_1}}\right]. \tag{2}$$

Here,

$$\chi_i = 3 - 4\nu_i \quad \text{for plane strain } (i = 1, 2). \tag{3}$$

The stress distribution near the crack tip is given by the following equation:

$$\begin{aligned}\sigma_y + \mathrm{i}\tau_{xy} &= \frac{K_1 + \mathrm{i}K_2}{\sqrt{2\pi r}} \left(\frac{r}{l_k}\right)^{\mathrm{i}\varepsilon} \\ &= \frac{K_1 + \mathrm{i}K_2}{\sqrt{2\pi r}} \left(\cos\left(\varepsilon \ln\left(\frac{r}{l_k}\right)\right) + \mathrm{i}\sin\left(\varepsilon \ln\left(\frac{r}{l_k}\right)\right)\right).\end{aligned} \tag{4}$$

The distribution of the displacement near the crack tip is also given by the following equation:

$$\delta_y + \mathrm{i}\delta_x = \frac{K_1 + \mathrm{i}K_2}{2(1 + 2\mathrm{i}\varepsilon)\cosh(\varepsilon\pi)} \left\{\frac{\chi_1 + 1}{\mu_1} + \frac{\chi_2 + 1}{\mu_2}\right\} \left(\frac{r}{2\pi}\right)^{1/2} \left(\frac{r}{l_k}\right)^{\mathrm{i}\varepsilon}. \tag{5}$$

K_1 and K_2 are complex stress intensity factors in the above equations.

Here, l_k is the reference length to normalize oscillation terms and has the value of 10 μm in this paper. Ikeda *et al.* stated that l_k of 10 μm could represent the mixed Mode interfacial fracture test data curve between epoxy and other materials as a partial ellipse [13]. They attributed this fact to the agreement of the process zone of epoxy with the length of l_k. Thus, this value was adopted in the analyses of this paper.

3.1.2. Determination of stress intensity factors and the energy release rate. Stress intensity factors, K_1, K_2, with higher accuracy, are suggested to be derived from the energy release rate, G, and the Mode ratio, K_2/K_1 [14].

Here, the Mode ratio of complex stress intensity factors, K_2/K_1, was calculated using a displacement method owing to the higher accuracy than a stress method in the analyses [15, 16].

K_2/K_1 is defined in the following equations:

$$K_2/K_1 = \lim_{r\to 0}\{1 - (\delta_y/\delta_x)H\}/(\delta_y/\delta_x + H), \tag{6}$$

$$H = (\tan Q - 2\varepsilon)/(1 + 2\varepsilon \tan Q). \tag{7}$$

Here, $Q = \varepsilon \ln(r/l_k)$ in the above equations.

Energy release rates are also given using the crack closure method [17] and are shown in equation (8), since the crack closure method gave a precise value of total energy release rates for mixed Mode condition.

$$G = \lim_{\Delta a\to 0} \frac{1}{2\Delta a}\int_0^{\Delta a} \sigma_y(\Delta a - r, 0)\bar{v}(r, \pi)\,\mathrm{d}r + \lim_{\Delta a\to 0} \frac{1}{2\Delta a}\int_0^{\Delta a} \tau_{xy}(\Delta a - r, 0)\bar{u}(r, \pi)\,\mathrm{d}r. \tag{8}$$

Here, G is energy release rates and σ_y, τ_{xy} are normal and shear stress components near the crack tip, respectively. $\bar{u}$ and $\bar{v}$ are the in-plane shear and vertical displacement between upper and lower crack surfaces, respectively. Δa is the crack extension.

Therefore, stress intensity factors, K_1, K_2, can be obtained from energy release rates and Mode ratio by the following equation:

$$G = \frac{1}{16\cosh^2(\varepsilon\pi)}\left\{\frac{\chi_1 + 1}{\mu_1} + \frac{\chi_2 + 1}{\mu_2}\right\}(K_1^2 + K_2^2). \tag{9}$$

3.2. Analysis Model and its boundary conditions

The effects of the crack arrester with different sizes and materials were evaluated for Mode I and Mode II loading conditions. Commercial FEM code of MSC Marc 2001 was used for two-dimensional large deformation plain strain elastic analyses. The suppression effect of the new crack arrester on the interfacial crack was estimated using fracture mechanical parameters as explained in 3.1. FEM analyses were conducted for the three different radii of the crack arrester, 2.5 mm, 5.0 mm and 10 mm. Two types of materials for the crack arrester, CFRP UD and epoxy resin, were evaluated. The changes of the energy release rates at the crack tip were investigated. Here, calculations were carried out where the crack tip locations were less than about 20 mm from the leading edge of the crack arrester. A typical mesh pattern of the crack arrester Model was shown in Fig. 6. Eight nodes isoparametric

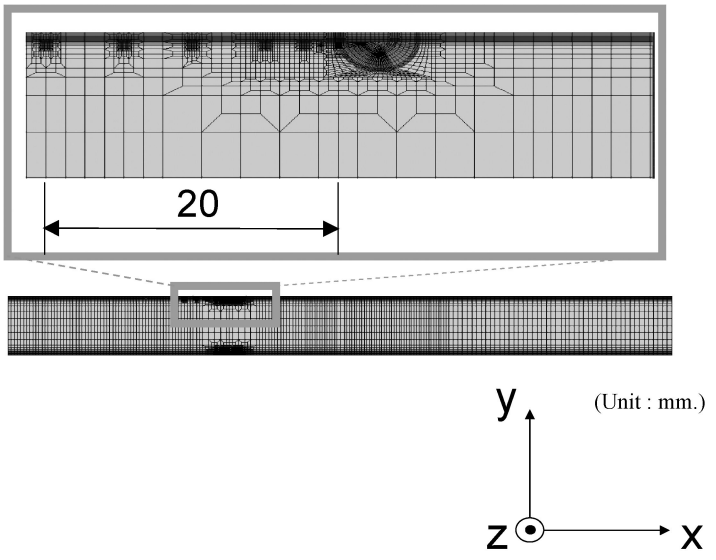

Figure 6. Typical FE Model for crack arrester ($R = 2.5$ mm).

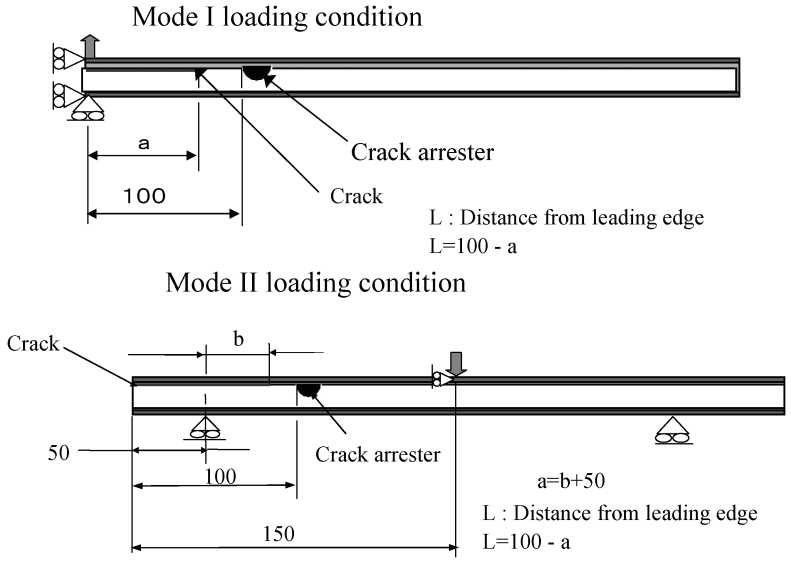

Figure 7. Schematic views of loading conditions.

elements were used in this figure. Schematic views of FE Model for Mode I and Mode II loading conditions were shown in Fig. 7.

In addition, the crack kinking for the ENF (End Notch Flexure) specimen and the arrester effect on the crack propagating beyond a leading edge were also investigated. The crack kinking in the foam core sandwich panel was expected under the Mode II loading condition because there were several studies on this

matter [18, 19]. Hence, the analysis of the crack kinking is necessary in this study. A schematic view of FE Models for crack kinking was shown in Fig. 8.

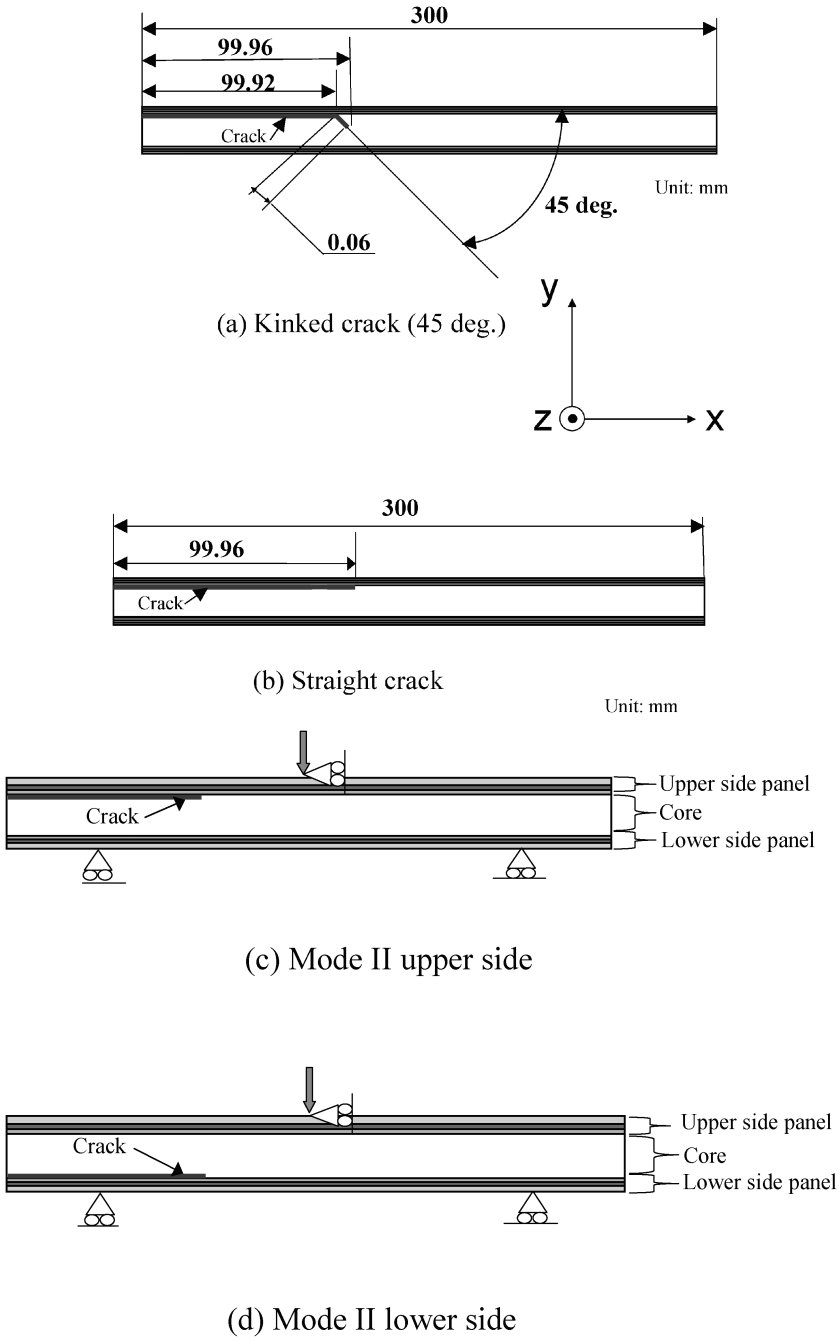

Figure 8. Schematic view of FE Model for kinked crack and straight crack.

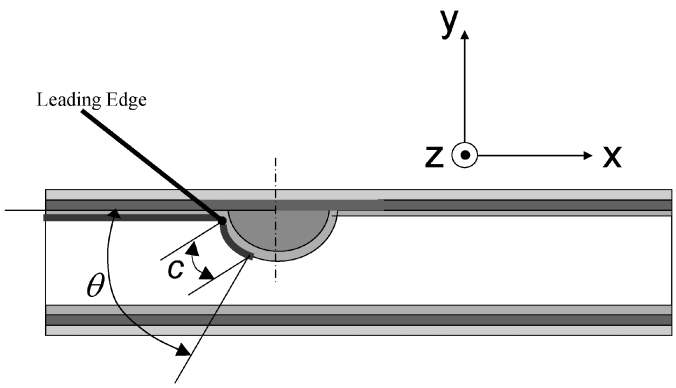

Figure 9. Schematic view of FE Model (beyond the leading edge).

It is also necessary to estimate the arrester effect when the crack propagated beyond the leading edge of the arrester owing to impact damage, etc. The crack located beyond the leading edge of the arrester, which is denoted as beyond the leading edge case, was considered to propagate along the circumference on the semi-cylindrical crack arrester as shown in Fig. 9.

4. ANALYTICAL RESULTS AND DISCUSSION

4.1. Investigation of crack propagation and kinking behavior

The crack kinking was first analyzed to focus the possible crack path. An initiation of the crack kinking depends on the ratio of Young's modulus for the surface skin and the foam core. In this study the energy release rates at the crack tip for the straight crack and the kinked crack were calculated and compared. Typical analysis Model of this comparison is shown in Fig. 8(a) and 8(b). The loading condition was 3-point bending and the applied load was 1500 N. The energy release rates were calculated and the results were compared in Table 2. The terms 'upper side' and 'lower side' referred to in Table 2 indicate the crack location on the side of a loading point and on the side of support points, respectively (see Fig. 8(c) and 8(d)). Thus, the same Model with a different loading point, and support points was used to obtain the energy release rates for both upper and lower side cases. The data in Table 2 indicate that the energy release rate at the straight crack tip is larger than that of the kinked one in the upper side case. On the other hand, the energy release rate at the kinked crack is larger in the lower side case. Thus, an initial crack in the upper side is expected to propagate along the interface. Only a crack location in the upper side was to be investigated in this study, because the crack on the lower side was kinked and finally reached to the upper side, and then propagated along the interface.

4.2. Arrester effects for Mode I case

The arrester effect is shown in Fig. 10. This effect is defined by the normalized energy release, G_{be}/G_0. Here, G_{be} is the energy release rate at the crack tip located

Table 2.
Effect of crack pass direction on energy release rate for Mode II case

	Lower side		Upper side	
	Straight crack	Kinked crack	Straight crack	Kinked crack
G (J/m^2)	2.70	4.67	2.52	2.13
F (N)	1500	1500	1500	1500

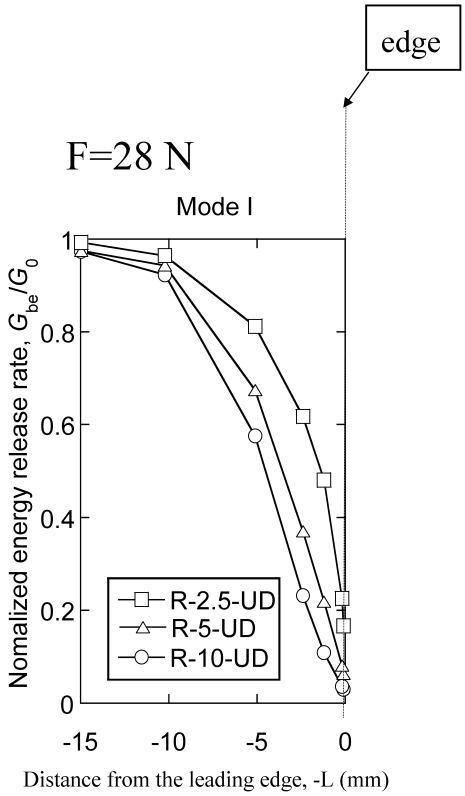

Figure 10. Relation between normalized energy release rate and distance L (Mode I, in front of the leading edge).

in front of the leading edge of the arrester and G_0 is the energy release rate without the arrester with the same crack length as that for G_{be}. It was shown in Fig. 10 that G_{be}/G_0 is simply decreased from 1.0 at $L = 15$ mm to the small value close to 0 at $L = 0.085$ mm. Here, L is the distance from the leading edge of the crack arrester. Thus, crack suppression effect of the new crack arrester was analytically evaluated with the fracture mechanical approach for the Mode I loading condition.

Individual stress intensity factors K_1 and K_2 for the distance from the leading edge of the crack arrester, L, are show in Fig. 11(a) for the detailed understanding of the effect of each Mode. The values of K_1 and K_2 decrease rapidly after the

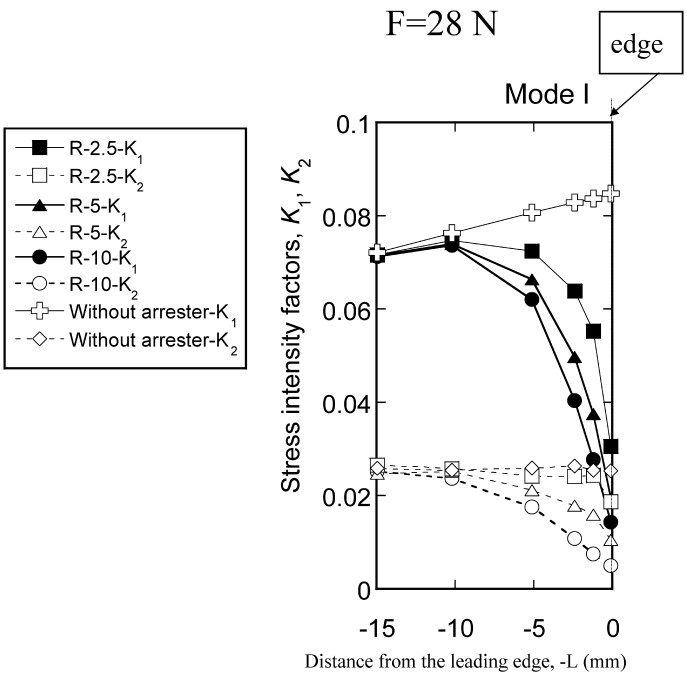

(a) Stress intensity factor K_2 and K_1

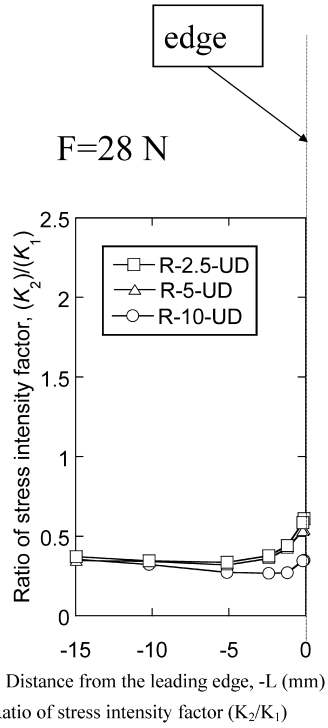

(b) Ratio of stress intensity factor (K_2/K_1)

Figure 11. Relation between of stress intensity factors and distance *L* (Mode I, in front of the leading edge).

point of $L = 10$ mm and the arrester with the larger radius has the larger reduction. The change of the ratio of the stress intensity factor, K_2/K_1, with the distance from the leading edge of the crack arrester, L, is also shown in Fig. 11(b). This ratio was almost constant as the crack propagated until $L = 5.1$ mm. After this point, the ratios of K_2/K_1 for all arrester sizes are increased. These facts indicate that the energy release rate is decreased owing to significant reductions of the Mode I component, K_1, regardless of R-values. This rapid reduction of Mode I component near the leading edge of the arrester causes the local increase of the Mode ratio shown in Fig. 11 though the Mode I component was still dominant.

4.3. Arrester effect for Mode II upper side case

The arrester effect under the Mode II loading is shown in Fig. 12. The definition of the arrester effect is the same as that in the Mode I case. It was shown in Fig. 12 that the reduction of G_{be}/G_0, starting after the point of $L = 20$ mm, became rapid after the point at $L = 10$ mm and the normalized energy release rates converged to a small value close to 0 at $L = 0.085$ mm. The crack suppression effect for the Mode II upper side case is clear in Fig. 12. This effect was higher for larger arrester radius. Individual stress intensity factors K_1 and K_2 for the distance from the leading edge of the crack arrester, L, are show in Fig. 13(a). The values of both

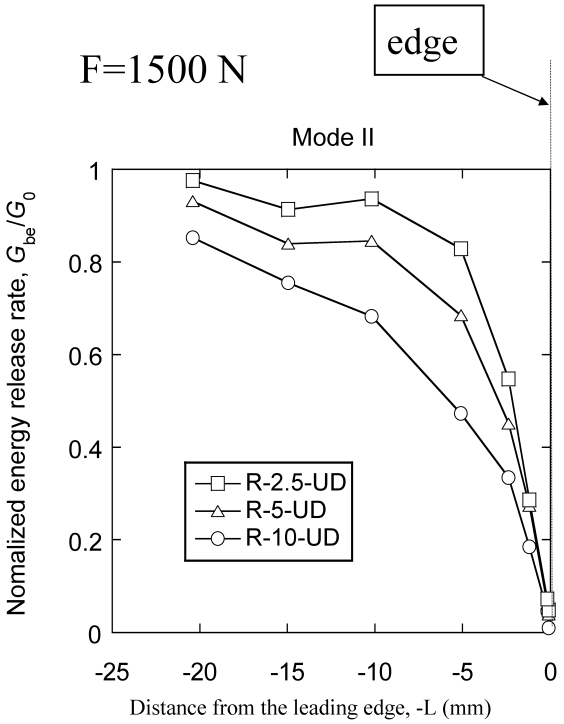

Figure 12. Relation between normalized energy release rate and distance L (Mode II upper side, in front of the leading edge).

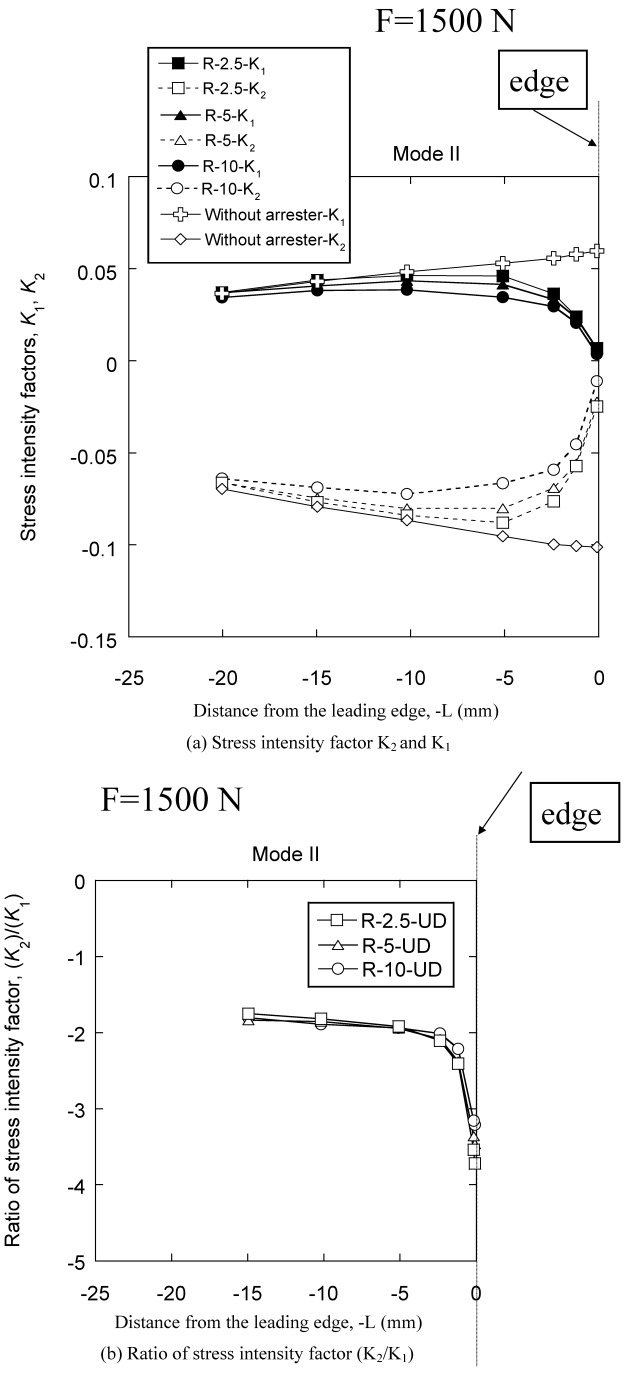

Figure 13. Relation between of stress intensity factors and distance L (Mode II upper side, in front of the leading edge).

K_1 and K_2 converged to a small value close to 0 at $L = 0.085$ mm. The change of the ratio of stress intensity factor, K_2/K_1, with the distance L is also shown in Fig. 13(b). It was revealed that the Mode II component is relatively dominant near the leading edge of the arrester and the ratio of the complex stress intensity factors, K_2/K_1, has little dependency on the R-value.

4.4. The difference of the arrester effect between Mode I case and Mode II upper side case

The arrester effect, indicated by the reduction of G_{be}/G_0, for the Mode II loading started at a further distance from the leading edge of the arrester than that for the Mode I loading (see Figs 10 and 12). From this point of view, the new crack arrester was more effective for the Mode II upper side case than for the Mode I case. The differences of stress distribution near the crack tip are shown in Fig. 14. The distribution of shear stress τ_{xy} was more dominant in the x-direction from the crack tip in the Mode II loading condition. On the other hand, normal stress σ_{yy} distribution was more dominant in the y-direction in the Mode I loading condition. The above results suggest that the constraint effect of the crack arrester is different between the Mode I case and the Mode II upper side case. A relatively small arrester has enough effect to suppress crack growth for the Mode II upper side case; however, for the Mode I case, the arrester effect is dependent on the arrester size owing to difference of the stress distributions shown in Fig. 14.

4.5. The effect of the mechanical properties of the arrester

The effect of the mechanical properties of arresters on the normalized energy release rate, G_{be}/G_0, is shown in Fig. 15 (for Mode I case) and Fig. 16 (for Mode II upper side case) for each arrester radius. The differences of the mechanical properties of the arrester ranging from those of the resin to the CFRP UD have little effect on the energy release rates reduction both under the Mode I case and the Mode II upper side case. This is due to the fact that the mechanical property, E_{22}, of the foam core was much less than that of the resin and the CFRP UD material of the order of 10^{-2} (See Table 1). The ratio of the complex stress intensity factor, K_2/K_1, has a similar trend as previous ones.

4.6. The arrester effect on the crack propagating beyond the leading edge

The analytical results are shown in Table 3. Here, G_{ae} is the energy release rate at the crack tip with the arrester for beyond leading edge case and G_0 is the energy release rate without the arrester for the same crack length as that for G_{ae}. The energy release rate reaches the maximum value at $\theta = 90$ degree and normalized energy release rate, G_{ae}/G_0, is less than 1.0 at this point. These results indicate that the new crack arrester is also effective in the beyond leading edge case. The configuration of the crack arrester should be sophisticated in order to avoid a stress singular point as a crack initiation point. This is a subject for a future study.

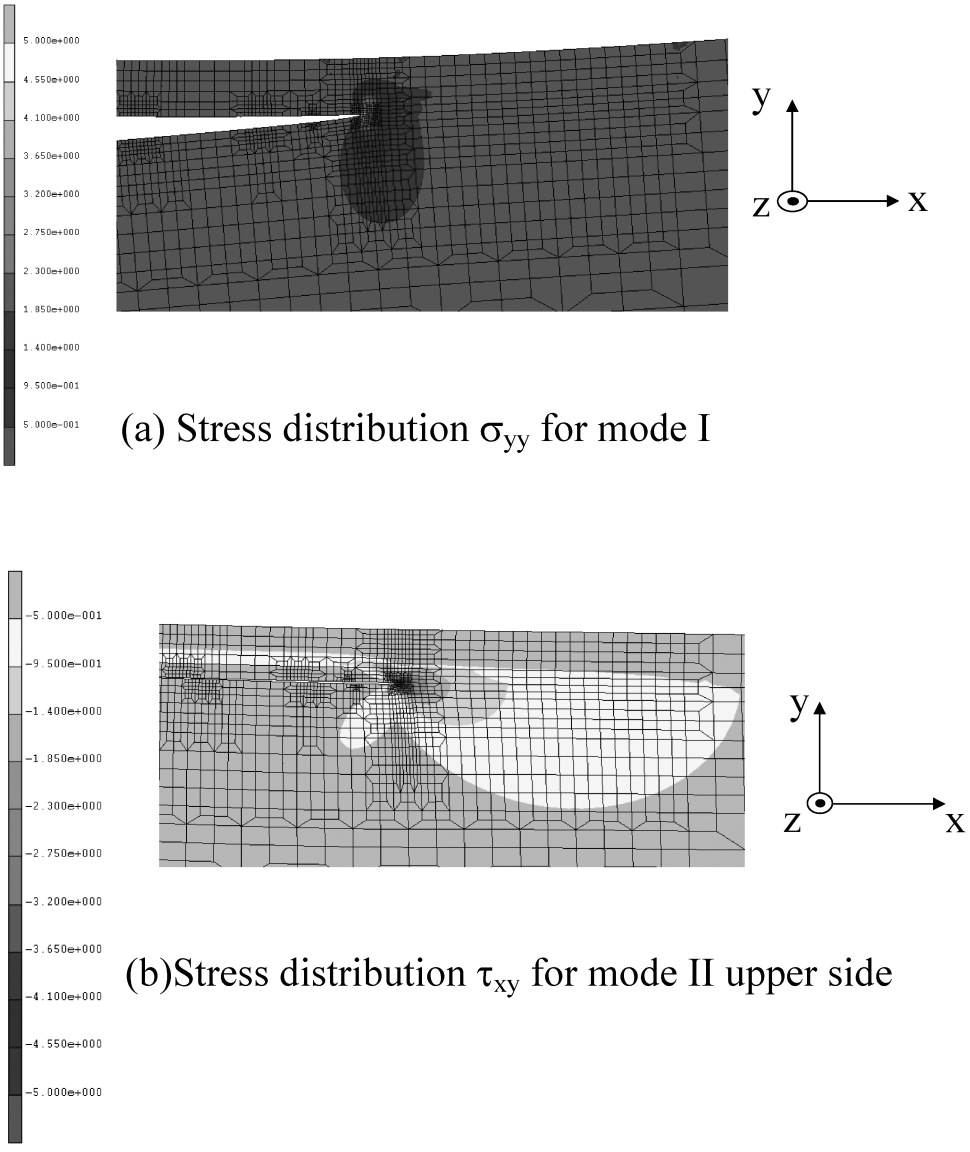

Figure 14. Difference of stress distribution near the crack tip for Mode I and Mode II loadings.

The present study considers only the concept of delamination suppression in a two-dimensional analysis. In the real application of aircraft structures, this new arrester will be practically arranged in a grid pattern, which should improve the damage tolerance capability of the co-cured sandwich panel structure, and this may in turn eventually lead to a new design concept for the next generation air transport.

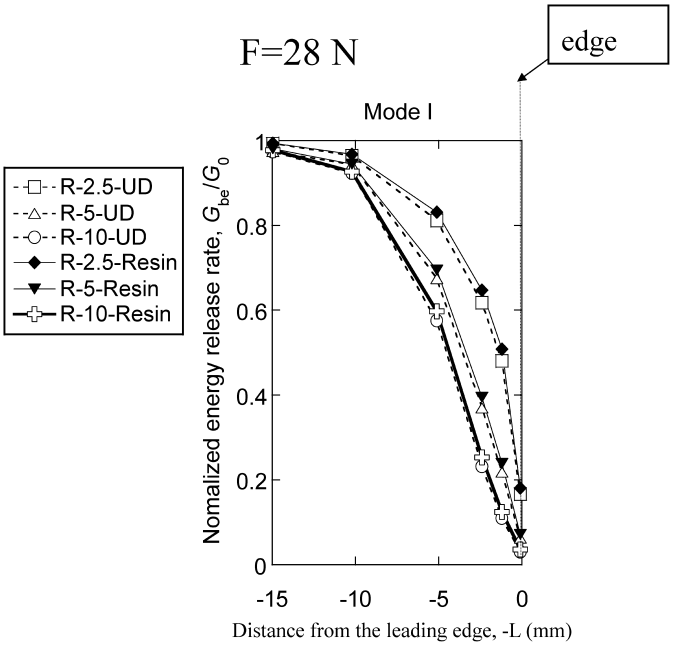

Figure 15. The effect of mechanical properties of crack arrester for Mode I (in front of the leading edge).

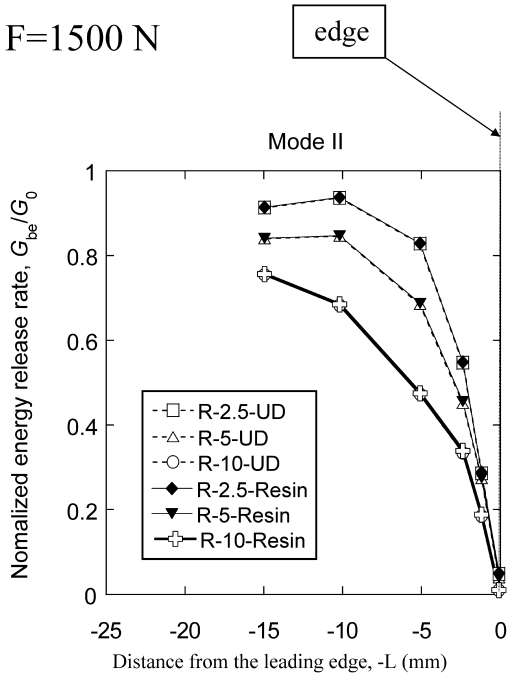

Figure 16. The effect of mechanical properties of crack arrester for Mode II upper side (in front of the leading edge).

Table 3.
Energy release rate for beyond leading edge condition ($\theta = 90$ deg.)

	Mode I			Mode II		
Load (N)	28			1500		
Arrester size	$R = 2.5$	$R = 5$	$R = 10$	$R = 2.5$	$R = 5$	$R = 10$
G_{ae} (J/m^2)	98.0	52.8	24.1	110.2	91.1	55.8
G_{ae}/G_0	0.86	0.44	0.18	0.47	0.36	0.19

5. CONCLUSION

The following results were obtained in this study.

(1) An interfacial crack propagated between the resin layer adjacent to the surface skin and the foam core for the Mode I and the Mode II upper side loading condition. Crack kinking was expected to initiate for the Mode II lower side case. The crack on the lower side was kinked and finally reached the upper side, and then propagated along the interface.

(2) The normalized energy release rate, G_{be}/G_0, decreased as a crack approached to the leading edge of the arrester for both the Mode I and the Mode II upper side loading. This arrester effect was more dominant for larger arrester radius. The arrester radius effect was more significant for the Mode I case than that for the Mode II upper side case.

(3) The arrester effect, G_{be}/G_0, for the Mode II loading started at a further distance from the leading edge of the arrester than that for the Mode I loading.

(4) Materials, with higher modulus than that of the foam core, are expected to have enough effect to suppress the crack propagation. This means that relatively cheap materials such as resins are available for the arrester and widespread usage of this concept in the industrial field are expected.

Acknowledgement

The authors would like to acknowledge their appreciation to Professor Toru Ikeda of Kyoto University for his valuable advice on the calculation method for the stress intensity factors.

REFERENCES

1. A. Fawcett, J. Trostle and S. Ward, 777 empennage certification approach, in: *Proc. ICCM11*, Gold Coast, Australia, pp. 178–199 (1997).
2. D. Schulz, Structural certification of Airbus fin box in composite fiber construction, in: *Proc 14th International Congress of Aerospace Sciences*, Toulouse, France, pp. 427–438 (1984).
3. S. Ochi, Y. Hirose, M. Nishitani, T. Sana, T. Ito, Y. Ikeda and H. Kikukawa, Development of CFRP sandwich panel structure for transport nose component, in: *Proc. 9th European–Japanese Symposium on Composite Materials*, Hamburg, Germany (2004).

4. Y. Ikeda, Y. Hirose, M. Nishitani, S. Ochi and T. Ito, Development of foam core sandwich panel structure for transport nose structure, in: *Proc. 5th Gyeongnam (Korea)-Tokai (Japan) Aerospace Technology Symposium*, Sacheon, Korea, pp. 67–78 (2004).
5. L. Herbec, Technology and design development for a CFRP fuselage, Presented at 25th SAMPE Europe Conference, Paris, France (2003).
6. M. Bruman, Fatigue crack initiation and propagation in sandwich structures, Report No. 98-29, Department of Aeronautics, Royal Institute of Technology, Sweden (1998).
7. A. Shipsha, Failure of Sandwich Structures with Sub-interface Damage, Report 2001-13, Department of Aeronautics, Royal Institute of Technology, Stockholm, Sweden (2001).
8. Y. Hirose, M. Konishi, K. Kosugi, M. Imuta and H. Kikukawa H, Industrial application of CFRP sandwich panel for aircraft structure, in: *Proc. Conference ICCM/8*, Tenerife, Canary Island, Spain, pp. 355–356 (2001).
9. S.-E. Hellbrantt, Experience from design and production of the 72 m CFRP-sandwich corvette Visby, in: *Proc.6th International Conf. Sandwich Struct.*, Ft. Lauderdale, Florida, pp. 15–24 (2003).
10. Y. Hirose, K. Kosugi, M. Nishitani, H. Sashikuma, M. Imuta, H. Fukagawa and H. Kukukawa, The CFRP sandwich panel for aircraft nose structure, in: *Proc. 23rd Int. Congress Aerospace Sci.*, Toronto, Canada, pp. 343.1–343.10 (2002).
11. Y. Hirose, H. Fukagawa, K. Kosugi, M. Imuta and H. Kikukawa, Application of a new CFRP sandwich panel to the aircraft nose structure, in: *Proc. 10th US–Japan Conf. Compos. Mater.*, Stanford University, USA, pp. 969–977 (2002).
12. T. Yuki, K. Kishimoto and J. Shu, *Mechanics of Interface*, Baifukan Co., LTD, Tokyo, pp. 91–96 (1993).
13. T. Ikeda and N. Miyazaki, Mixed mode fracture criterion of interface crack between dissimilar materials, *Engng Fract. Mech.* **59**, 725–735 (1998).
14. T. Ikeda and C. T. Sun, Stress intensity factor analysis for an interface crack between dissimilar isotropic materials under thermal stress, *Int. J. Fract.* **111**, 229–249 (2001).
15. W. Qian and C. T. Sun, Calculation of stress intensity factors for interlaminar cracks in composite laminates, *Compos. Sci. Technol.* **57**, 637–650 (1997).
16. Y. Matsushita, The study of the interfacial fracture mechanism for GE/Epoxy with the modified couple fiber method, Master degree thesis, Dept. of Mechanical Engineering and Science, Kyoto University (2005).
17. E. F. Ryubicki and M. F. Kanninen, A finite element calculation of stress intensity factors by a modified crack closure integral, *Eng. Fract. Mech.* **9**, 931 (1977).
18. S. Prasad and L. Carlsson, Debonding and crack kinking in foam core sandwich beam – I. Analysis of fracture specimens, *Engng. Fract. Mech.* **47**, 813–824 (1994).
19. S. Prasad and L. Carlsson, Debonding and crack kinking in foam core sandwich beam – II. Experimental investigation, *Engng. Fract. Mech.* **47**, 825–841 (1994).